JMEPEG (2006) 15:102-110
DOI: 10.1361/105994906X83466

1059-9495/$19.00

Corrosion Wear Behavior of Al-Bronzes in 3.5% NaCl Solution

W.S. Li, Z.P. Wang, Y. Lu, and L.H. Yuan

(Submitted July 7, 2005; in revised form September 9, 2005)

The corrosion wear behaviors of two aluminum bronzes, Cu-14Al-X and QAl9-4, in 3.5% NaCl solution were investigated on a pin-on-block reciprocating tester. It was found that the wear loss of the bronzes in 3.5% NaCl solution was lower than that in water and in air, i.e., it exhibited "negative" synergy between corrosion and wear. To understand the corrosion wear mechanism of the bronzes, the corrosion rate and polarization curves of Cu-14Al-X and QAl9-4 in 3.5% NaCl solution were determined. The worn surfaces of the specimens were examined, and the wear tracks were measured using scanning electron microscopy. The corrosion patinas formed on the specimen surfaces were studied with x-ray photoelectron spectroscopy and electron probe microanalysis. The corrosive solution was shown to play an important role in cooling of the specimen surfaces during the wear, thus preventing the specimen's surface hardness from being reducing, induced by frictional heat during the sliding wear. On the other hand, the bronzes suffered from dealloying corrosion; a noble copper subsurface and patina formed on the specimen surface in the corrosive solution, which had a passive function for further corrosion. The noble copper subsurface experienced strain hardening during the corrosion wear, resulting in an increase of the surface hardness and thus an increase in wear resistance.

Keywords aluminum bronze, corrosion, corrosion wear, hardness, patina, strain hardening

1. Introduction

Copper (Cu)-based alloys are commonly used in saline water systems, e.g., heat exchangers and distillation-type desalination components. Among Cu-based alloys, aluminum (Al) bronzes are used extensively because they possess superior properties such as high strength, oxidation and corrosion resistance, abrasion, wear, cavitation and erosion resistance, and impact resistance (Ref 1-6).

Bronze alloyed with about 10% Al (in weight) exhibits the best comprehensive properties and is the most widely used material among the aluminum bronze family. Conventional bronze-10% Al alloys are ZQAl10-3-1.5 and ZQAl9-4, and their tribological behaviors have been studied extensively since the 1970s (Ref 2-5, 7). Shi et al. (Ref 8) and Blau (Ref 9) reported that, with increasing aluminum content up to the Cu-Al binary alloy's solubility limit (9.4 wt.%), the friction coefficient decreased but the wear loss increased when wearing against steel. A high-strength wear-resistant complex aluminum bronze, designated as Cu-14Al-X, with a 14-16 wt.% aluminum content, was developed by adding several trace elements, such as Zn, Co, RE (rare earth), and so on. This alloy exhibited a lower wear rate and friction coefficient and better anti-friction properties than the currently used aluminum bronzes ZQAl10-3-1.5 and ZQAl10-4-4 (Ref 10).

The corrosion behavior of copper and bronzes with an aluminum content less then 9.4 wt.% in various solutions has also been studied extensively. Ashour et al. (Ref 11, 12) reported the corrosion resistance of αAl bronze was attributed to the formation of a thin layer of alumina (Al_2O_3) in saline water, which protected the substrate alloy from further corrosion. They found stress-corrosion cracking (SCC) of single phase α-aluminum bronze in 3.4% NaCl solution and explained the result as a dealloying process occurred through a film of CuCl. Parkins et al. (Ref 13) found that complex α/β/κ nickel-aluminum bronzes were susceptible to cracking in natural seawater in monotonic strain rate cracking or cyclic loading tests, near the corrosion potential. Ateya et al. (Ref 2, 3) reported that α-aluminum bronze suffered from a dealuminum corrosion in saline water, and the α, β, and γ_2 phases exhibited different degrees of resistance to dealuminum corrosion in sodium chloride solution. The α phase was more stable than the β and γ_2 phases. Li et al. (Ref 14-16) studied the corrosion wear behav-

W.S. Li, Z.P. Wang, Y. Lu, and **L.H. Yuan,** State Key Lab of Advanced Non-Ferrous Materials, Lanzhou University of Technology, Lanzhou, Gansu, P.R. China 730050. Contact e-mail: Wensheng-li@sohu.com.

Table 1 Composition, strength, and hardness of the tested specimens

Alloy	Chemical composition, mass%							Tensile strength, MPa	Hardness
	Cu	Al	Fe	Mn	Ni	Co	Traces		
Cu-14Al-X	Bal	14-16	2.0-4.0	0.8-1.0	0.4-0.8	0.5-1.2	0.6-1.6	630	HRC 37
QAl9-4	Bal	8.0-10	2.0-4.0	…	…	…	…	430	HB 192

iors of brass in a mixed solution of 3.5% NaCl with sulfide or ammonia and/or ammonium. The results showed that the addition of ammonia and/or ammonium or sulfide could enhance the corrosion and corrosion wear of brass. This was attributed to the surface embrittlement induced by ammonia and/or ammonium or sulfide. Although research has been done on aluminum bronzes, no reports on their corrosion wear have been published up to now.

The objective of this research was to investigate and understand the corrosive wear of the newly developed Cu-14Al-X alloy, which has an higher aluminum content over the Cu-Al binary alloy's eutectoid limit (11.8 wt.%), and the commercial bronze QAl9-4 alloy in 3.5% sodium chloride solution. The corrosion rate and polarization curves of Cu-14Al-X and QAl9-4 in 3.5% NaCl solution were determined. The worn surfaces of the specimens were studied with scanning electron microscope (SEM). The corrosion patinas formed on the specimen surfaces were analyzed with x-ray photoelectron spectroscopy (XPS) and electron probe microanalyzer (EPMA).

2. Experimental Details

2.1 Material Fabrication

The experimental materials are the newly developed Cu-14Al-X and the commercial QAl9-4 bronzes, the chemical composition of the experimented materials are given in Table 1. The QAl9-4 bronze was used for comparison.

The Cu-14Al-X specimens were prepared by a single charging melting technique due to the high aluminum and complex content. The raw materials were pure copper (purity ≥ 99.95 wt.%), aluminum (purity ≥ 99.9 wt.%), electrolytic nickel (purity ≥ 99.95 wt.%), manganese (purity ≥ 99.95 wt.%), zinc (purity ≥ 99.95 wt.%), cobalt (purity ≥ 99.95 wt.%), and cerium (purity ≥ 99.95 wt.%). In addition, deoiled iron scraps with polished surfaces and trace element limits, C wt.% < 0.04, Si wt.% < 0.03, P wt.% < 0.05, and S wt.% < 0.03, were used to provide ferrous ingredients for the alloy.

In the preparation process, raw materials, Cu and Al, which have low and high melting points, respectively, were charged into the furnace successively. Trace additives such as Co, Ni, Fe, and Mn fragments were then inserted uniformly into the gaps between copper and aluminum pieces. Furthermore, ~5 wt.% Al of the entire aluminum content in the alloy's composition (listed in Table 1) acted as pre-deoxygenating and temperature-tuning reagents. After all of the raw materials were charged into the furnace, the furnace was preheated for 5-8 min using a low heating rate to exclude the oil and gas on/in the rare materials surface, and then a high heating rate was used to melt all materials as quickly as possible. After all of the raw materials were completely melted, a layer of charcoal 20-30 mm thick was used to cover the molten surface. During the processing, a blowing device was used to perform dynamical degassing; the inert gas used for dynamical degassing was nitrogen or argon. After dynamical degassing, a process of predeoxygenation was carried out using the residual ~5 wt.% Al. In the mean time, the melting temperature was adjusted to 1200-1260 °C. A chemical refining degas procedure was then performed using the C_2Cl_6 and/or C_2Cl_4 refining reagents with an amount of 0.1-0.15% of all the molten materials (by weight). Afterward, an eventual deoxygenation process was taken using rare earth (RE). Before the pouring process, the gas was checked to ensure that it met the required criteria (Chinese standard GB/T 1176-1987). Finally, the previously melted materials were poured into sand moulds at 1180-1240 °C.

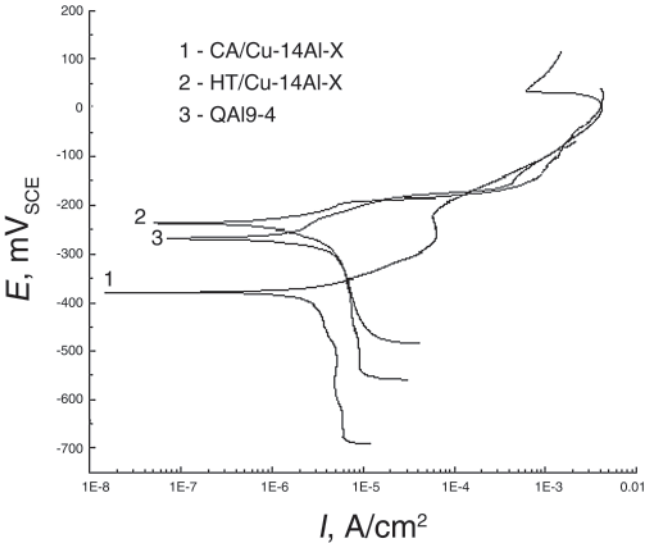

Fig. 1 Polarization curves of bronzes in 3.5% NaCl solution

Table 2 Corrosive rate of bronzes in 3.5% NaCl solution at 18 °C

Bronzes	CA/Cu-14Al-X	HT/Cu-14Al-X	QAl9-4
Corrosive rate, $gm^{-2}h^{-1}$	0.0264	0.0258	0.026

The developed alloy in its as-cast state (CA) was also heat treated. The heat-treated specimens (HT) were solution treated at 920 °C for 3 h and then aged at 580 °C for 5 h. The HT/Cu-14Al-X (heat-treated) bronze has a hardness of 39-41 HRC and a tensile strength of about 657 MPa.

2.2 Hardness, Corrosion, and Corrosion Wear Tests

Rockwell and Vicker hardnesses of Cu-14Al-X and QAl9-4 specimens were tested on the HD1-187.5 sclerometer and HVS-100 digital microhardness tester, respectively. The high-temperature hardness of the specimens was also measured with a thermoelectric couple heated by radiant energy.

The steady-state corrosion rate was measured by an immersion test. Specimens were machined and polished with emery papers up to 1200 grit. All tests were carried out at room temperature (~18 °C). Corrosion loss was calculated by measuring the weight loss of the specimen using a balance with a resolution within 0.1 mg in terms of standard criteria (Chinese standard GB 10124-88).

Electrochemical investigations were performed on an M263 apparatus. The electrode was a bronze specimen, and it was isolated by a polytetrafluoroethylene (PTFE) band from an aggressive environment, leaving a working area of 10 mm^2. The potential of the working bronze electrodes was measured with respect to a saturated calomel electrode (SCE) and a Luggin capillary. The counter electrode was a platinum electrode. Polarization curves were obtained by a potentiodynamic method with a scanning rate of 5 mV/min from free potential to −300 mV at the cathode. They were converted to 300 mV in anodic polarization relative to E_{corr}.

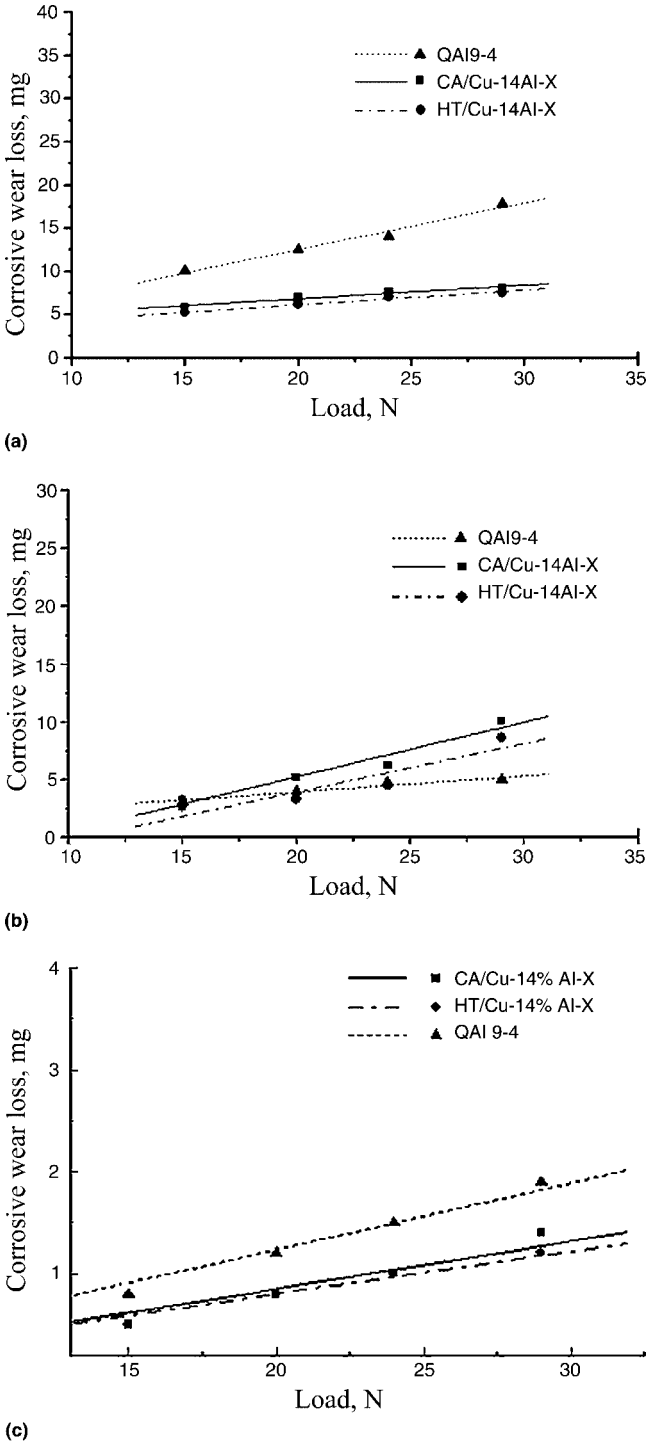

Fig. 2 Curves of wear losses with load: (a) dry; (b) pure water; (c) 3.5% NaCl solution

A pin-on-block reciprocating tester was used to measure the corrosion wear rate and friction coefficient of the specimens in 3.5% sodium chloride (NaCl) solution. The pin was a ceramic silicon nitride (Si_3N_4) ball with 6 mm in diameter. The corrosion wear loss was obtained by calculating the volume of the wear track after the specimen surface was worn for 120 min, which corresponded to a sliding distance of about 480 m. The wear load varied from 15 to 29 N. The volume of the wear track was the product of the sliding distance and the cross-sectional area, which was an average of six equidistant positions.

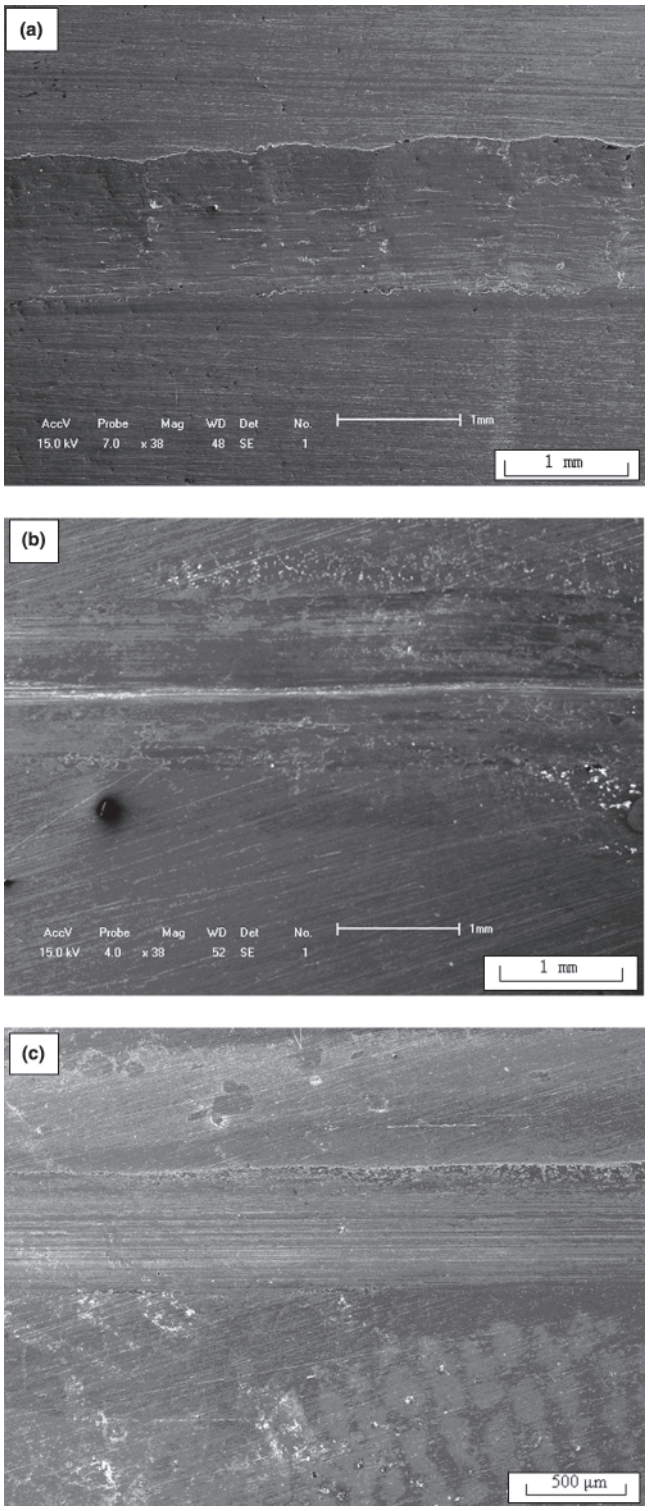

Fig. 3 Worn surface of as-cast Cu-14Al-X alloy (24 N): (a) dry; (b) pure water; (c) 3.5% NaCl solution

2.3 Worn Surface Examination

The topographical features and microconstituents of the worn surfaces and debris of the specimens were analyzed using the SEM, EDS, and EPMA. The surface-sensitive techniques, such as x-ray photoelectron spectroscopy (XPS), were used to investigate the composition of these ultra-thin layers that formed during the corrosion wear process.

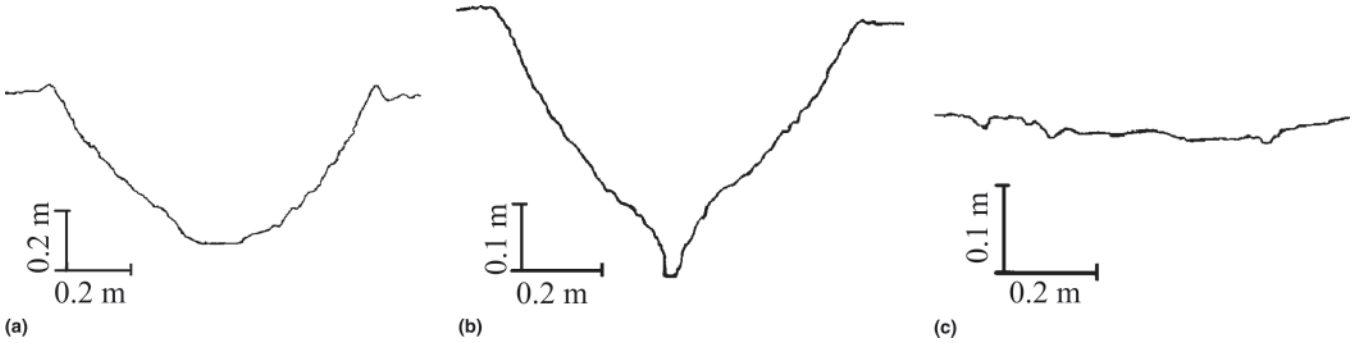

Fig. 4 Cross-sectional traces of the scratch grooves for as-cast Cu-14Al-X alloy (24 N): (a) dry; (b) pure water; (c) 3.5% NaCl solution

3. Experimental Results

3.1 Static Corrosion

Figure 1 shows the potentiodynamic polarization curves of the tested specimens in 3.5% sodium chloride solution at room temperature. One may see that the CA/Cu-14Al-X (as-cast) specimen has the highest corrosion rate, followed by the QAl9-4 specimen. The HT/Cu-14Al-X (heat-treated) specimen has the lowest corrosion rate. To further study the corrosion behavior of the alloys, the corrosion weight loss of the specimens was also measured, and the results are presented in Table 2. The HT/Cu-14Al-X specimen has the lowest weight loss, that is, the highest corrosion resistance, followed by the QAl9-4 specimen; the CA/Cu-14Al-X specimen has the highest weight loss. Therefore, HT/Cu-14Al-X is most noble and has the lowest anodic current density among the three alloys, i.e., HT/Cu-14Al-X is most resistant to static corrosion.

3.2 Corrosion Wear Resistance

Figure 2 shows the relationships between corrosion wear loss and load in air, pure water, and 3.5% sodium chloride solution, respectively. The corrosion wear loss in all media increases with the load and exhibits linear relationships.

The worn surfaces of the CA/Cu-14Al-X specimen under the load of 24 N in air, pure water, and 3.5% sodium chloride solution, respectively, are shown in Fig. 3. The cross-section profiles of the wear tracks are shown in Fig. 4. It can be seen that the worn surfaces in Fig. 3(a) and (b) are characterized by obvious plastic flows; in Fig. 4(a) and (b), the depths of the wear tracks are much deeper than that of the worn surface in 3.5% sodium chloride solution (Fig. 4c).

Figure 5 shows the debris collected from the worn surface of the HT/Cu-14Al-X specimen under a load of 24 N in air, pure water, and 3.5% sodium chloride solution medium. The debris from the worn surface in air is larger than those in pure water and 3.5% sodium chloride solution. The pieces of debris are nub-shaped, and cracks are found in them. However, the debris from the worn surface in pure water and 3.5% sodium chloride solution is small and granule-shaped, and its amount is also less, compared with that in dry sliding.

3.3 Friction Coefficient

The friction coefficients of the specimens in the corrosion wear were also measured, and the results are presented in Fig. 6. The friction coefficients in all media are shown to decrease with the load and exhibit a linear relationship; except for the CA/Cu-14Al-X specimen in 3.5% sodium chloride solution (Fig. 6c), the friction coefficient is nearly constant. This is in good agreement that CA/Cu-14Al-X has low corrosion resistance and low deformation resistance due to the nonhomogeneous microstructure in cast state (Ref 10).

Figure 7 shows the friction coefficients of the QAl9-4 and HT/Cu-14Al-X specimens in air, under cooling, and in a water pool, respectively. Cooling here means that the block specimen is placed in water with the specimen's surface in air, and water pool means that the whole specimen is immersed into water in a pool during sliding wear. For QAl9-4, the friction coefficient in dry sliding is the lowest, while it is the highest when the specimen is immersed in water with a wet surface (Fig. 7a). The same trend is observed with Cu-14Al-X (Fig. 7b).

3.4 Macro- and Microhardness

Variations in specimen hardness with temperature are presented in Fig. 8. The hardness of all specimens is shown to decrease with temperature.

The surface hardness of the region around the wear track was also measured. Figure 9 presents the microhardness of the areas inside and outside of the wear track on the HT/Cu-14Al-X specimen surface. It is shown that the hardness inside the wear track is higher than that outside the wear track, which indicates that strain hardening of the material occurred during the corrosion wear test.

3.5 Compositions of the Worn Surface Layers

The survey XPS spectra measured for HT/Cu-14Al-X in 3.5% NaCl solution are shown in Fig. 10. The copper and chlorine peaks are apparent, but aluminum and iron peaks are hardly visible. It is evident that the main element in the surface layer is copper.

The region of the Cu 2p peaks is shown in Fig. 11(a); the Cu 2p BE (932.5 eV) and BE (952.3 eV) demonstrate that Cu and Cu^{2+} compounds are the major constituents in the worn surface layer. Moreover, two shoulders are visible on the BEs (944.1 and 964 eV) of the Cu 2p peak, which indicates that the Cu^{+} component exists in the layer (Ref 17, 18). Therefore, components corresponding to different chemical states of copper exist in the worn surface layer. The Cl 2p peak is located at (198.6 and 200.4 eV) (Fig. 11b) and shows the presence of Cl^{-}, which is attributed to copper chloride (Ref 17, 18).

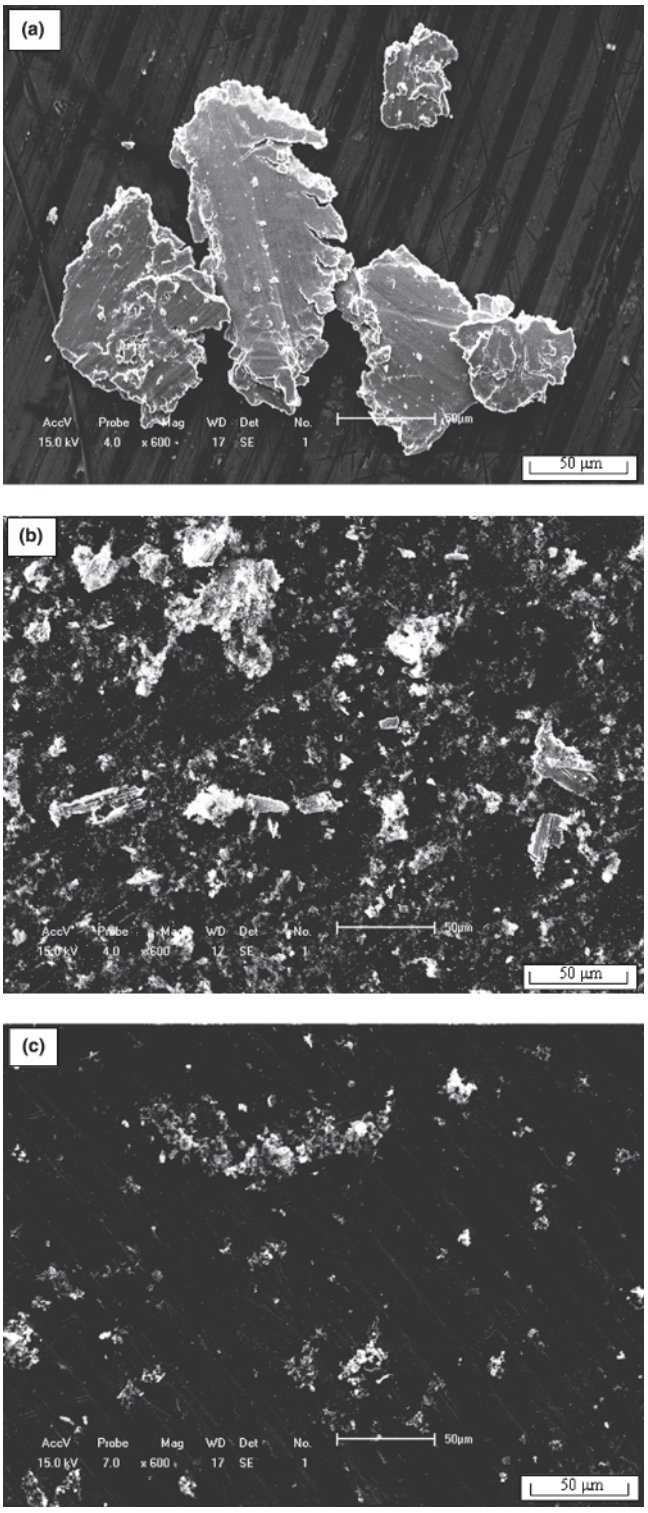

Fig. 5 Morphologies of wear debris of HT/Cu-14Al-X alloy (24 N): (a) dry; (b) pure water; (c) 3.5% NaCl solution

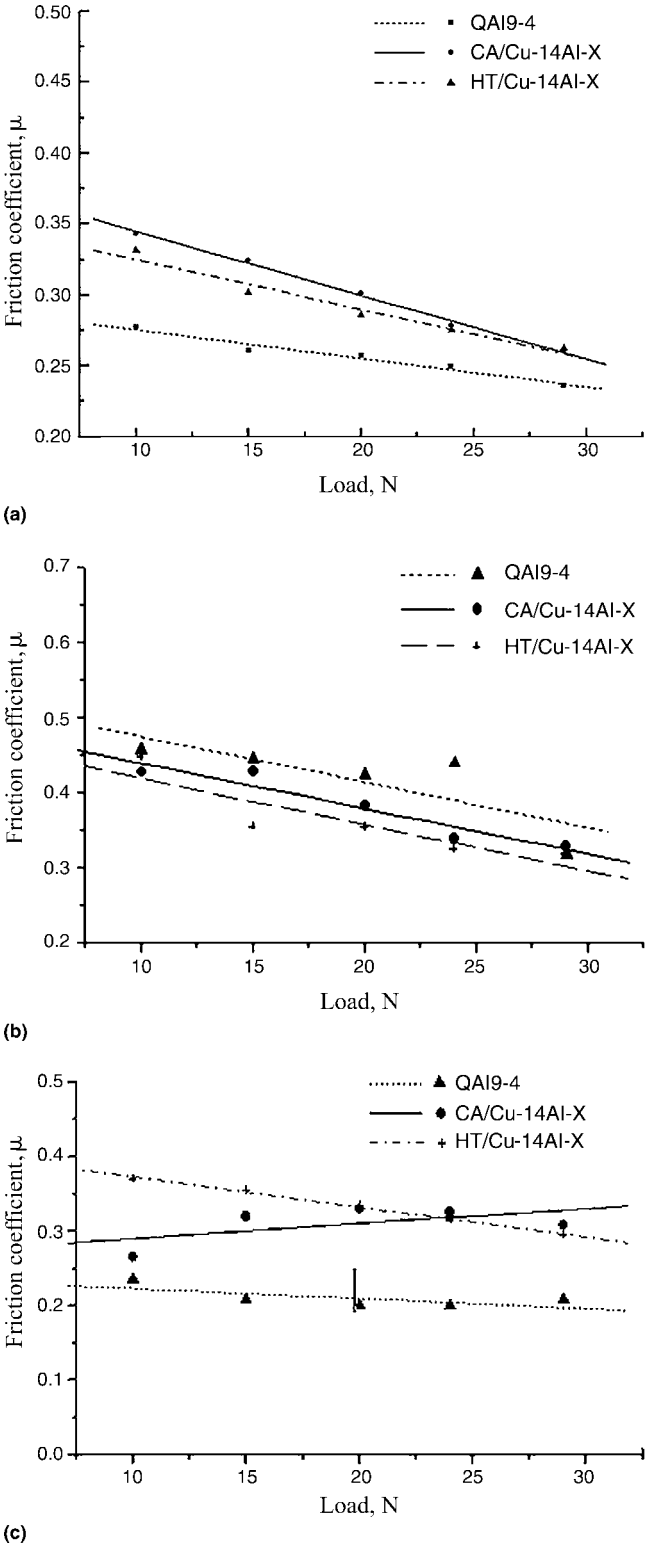

Fig. 6 Friction coefficient with load of the studied bronzes under no lubrication: (a) dry; (b) pure water; (c) 3.5% NaCl solution

4. Discussion

4.1 Wear Mechanisms

Sliding wear of a material in noncorrosive conditions depends on properties of the material, the applied load, and the contact geometry. Because the normal engineering-finished surfaces consist of asperities, when two surfaces come into contact, normal and tangential loads are transmitted through the contact points (Ref 4, 5, 7, 8). A series of experimental studies and the delamination theory of wear (Ref 19) have demonstrated that, as the asperities are gradually deformed and removed, the subsurface undergoes plastic deformation and the maximum plastic strain occurs right beneath the contact region.

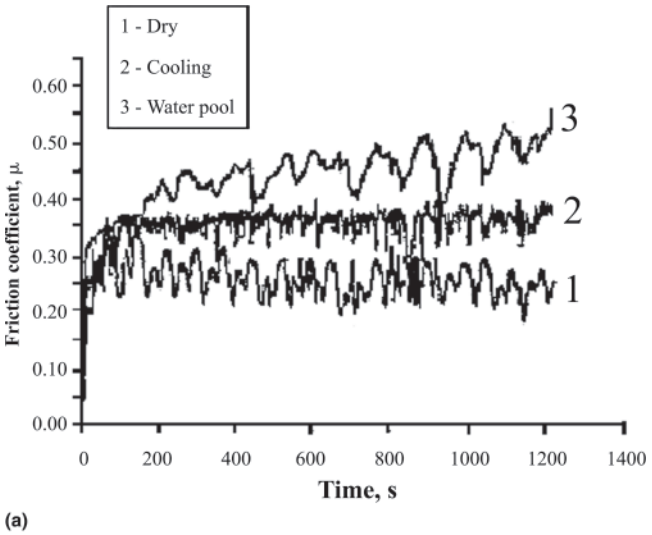

(a)

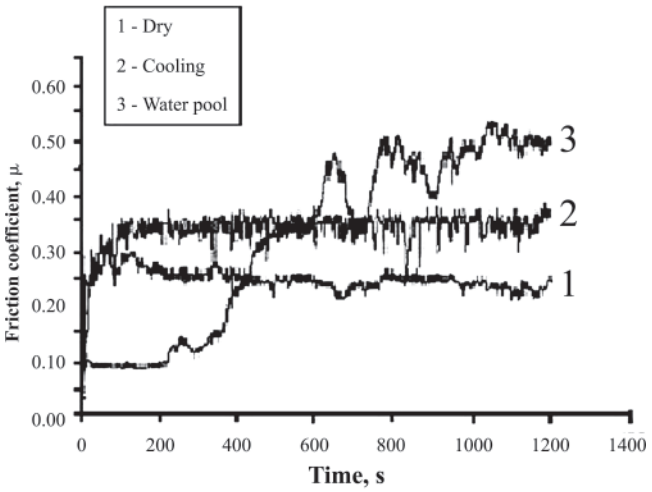

(b)

Fig. 7 Friction coefficient of bronzes in various mediums: (a) QAl9-4; (b) HT/Cu-14Al-X

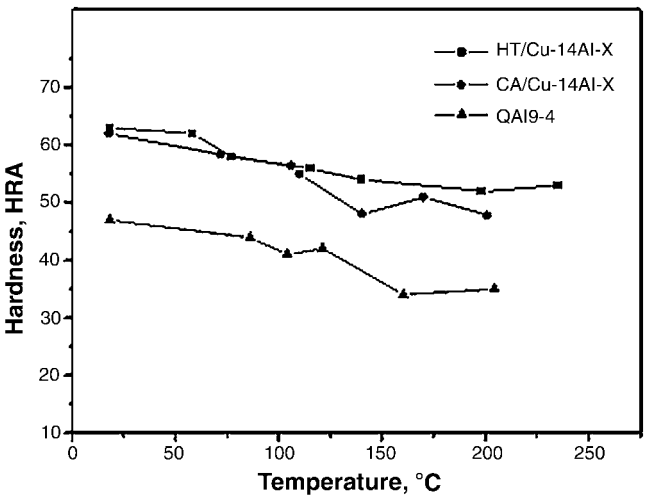

Fig. 8 Hardness with temperature of studied bronzes

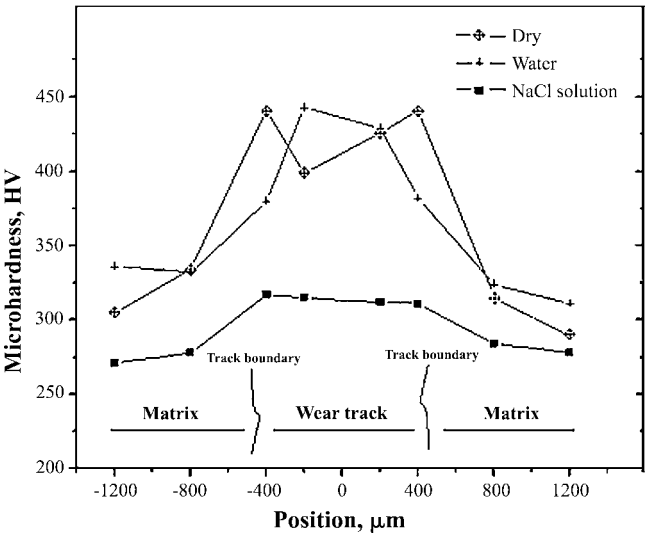

Fig. 9 Microhardness of HT/Cu-14Al-X bronze outside and inside grooves of corrosion wear

As the plastic strain accumulates and reaches the fracture strain of the material, cracks are nucleated below the surface and then propagate, leading to the material delamination at the surface. As shown in Fig. 5(a), the debris from the worn surface in dry sliding are large, nearly platelike particles and contain cracks. The wear characteristics of a material in dry sliding state are plow, delamination, and oxidation. Oxide scales can be seen in the surface by the naked eye. Generally, wear loss increases linearly with wear load.

In pure water, all of the specimens exhibit slightly lower weight losses, compared with experiments carried out in air, but higher friction coefficients (Fig. 2 and 6). This occurs because pure water has no lubrication effect on the contact surfaces. Thus plow and delamination are still observed in the worn surface, except that surface oxidation is reduced.

In sodium chloride solution, the wear tracks on the worn surface are shallower than in dry or water sliding wear, and the wear debris are smaller. There is no transverse microfracture in the corrosive wear surfaces (Fig. 3 and 4), which implies that no embrittlement was caused by the corrosive solutions and the bronzes only suffered from the mechanical attack of wear (Ref 14-16).

4.2 Friction Coefficients

Figure 6 shows that the friction coefficients in all media decrease with the wear load in the range 5-29 N and exhibit a nearly linear relationship. In pure water, the specimens have the highest friction coefficient under the same load. This may be due to the fact that pure water has no lubrication effect on the bronze/ceramic (Si_3N_4) counterparts. In dry sliding, oxide scale, e.g., CuO or Al_2O_3, may be formed on the specimen surface, which results in a low friction coefficient (Ref 7, 8, 20, 21). In sodium chloride solution, the corrosion products (CuCl, $[CuCl_2 \cdot 3Cu(OH)_3]$, $Al[OH]_3$, etc.) may also have a lubrication effect on the bronze/ceramic (Si_3N_4) counterparts, because the corrosion products have lower shear strength and are easy to remove from the contact surface (Ref 2, 3, 20, 21).

As presented in Fig. 7, for QAl9-4, the friction coefficients are stable within 2 min; the friction coefficient in dry sliding is the lowest, while that in water with a wet surface is the highest. The rubbing surfaces in dry sliding have a higher temperature than those immersed in water, and this promotes the formation

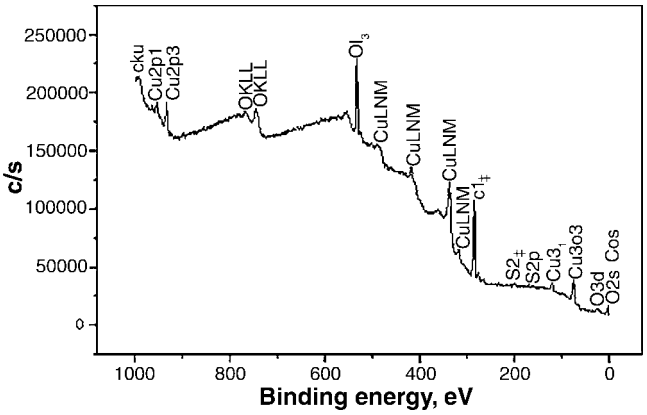

Fig. 10 Survey XPS spectra for HT/Cu-14Al-X in NaCl solution

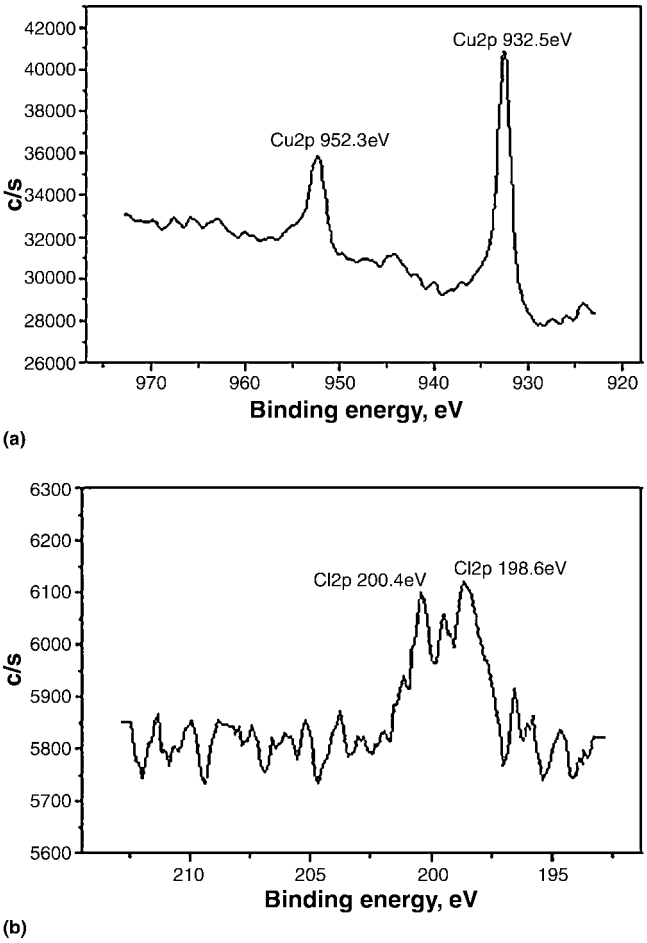

Fig. 11 XPS spectra for HT/Cu-14Al-X surface film in NaCl solution: (a) Cu 2p; (b) Cl 2p

of oxide scales on the dry-sliding worn surfaces. The brittle and fragile oxide scales lead to a lower friction coefficient (Ref 20-23). With Cu-14Al-X, the friction coefficients become stable within 2 min, but in the water pool wear condition, the friction coefficients become stable after the surface is worn for 12 min. Due to the high aluminum content in Cu-14Al-X, which is active in forming alumina and CuO films, the alloy has a low friction coefficient in air, but oxide films are not easy to form in the water pool cooling condition.

4.3 Negative Synergy between Corrosion and Wear

The synergism of wear and corrosion has become an important research area and has attracted increasing interest (Ref 14-16). The synergistic attack of wear and corrosion to metals is not well understood because it involves several simultaneous processes, such as formation and failure of passive films or adsorption layers, stress-accelerated corrosion, and corrosion-accelerated wear. However, a negative synergy between corrosion and wear may occur in the situation where the corrosive medium is very weak. In this case, material loss is caused mainly by wear and corrosive loss would be ignored. On the other hand, the corrosion products may change the surface contact state; for example, they may play a role as lubricant and the corrosive medium cools the specimens being worn. These may all contribute to reduction of material loss.

As illustrated in Fig. 2, the wear losses of the specimens in pure water are slightly lower than those in air, but they are much higher than those in 3.5% sodium chloride solution. This may be caused by a negative synergy effect between corrosion and wear.

As seen in Fig. 3 and 4 as well as in Table 3, the corrosive wear rate E_w is much higher than the corrosion rate E_c, therefore, wear dominates the corrosive wear process of the specimens in wet water or sodium chloride solution. The wear loss was predominant in the corrosive wear of the ZQAl10-3-1.5 and ZQAl9-4 alloys. In other words, corrosion wear is mainly a mechanical attack process.

The lubrication and cooling effects of the media can be another contribution to the low wear loss. In general, pure water has no or negligible corrosion to bronzes so that it is reasonable that the corrosive wear loss in 3.5% sodium chloride solution is higher than that in pure water. However, the experimental results obtained from this study are in contradiction with the convention. It is presumed that this is because frictional heat and corrosion patinas played an important role in corrosion wear of bronzes in 3.5% sodium chloride solution.

4.4 Effects of Frictional Heat on Corrosion Wear

In general, wear resistance of a material is proportional to its hardness (Ref 5, 22, 23), As presented in Fig. 8, the hardness of the specimens decreases with the temperature. In consistent with the wear results (Fig. 2), the wear resistance of the specimens is higher in water and in the solution than in air, because more frictional heat is generated in dry sliding and the frictional heat can be dissipated in water and in the solution. This agrees with the tribology theory of Rabinowicz and Archard (Ref 5, 22, 23): the lower the frictional heat, the higher the hardness is, leading to lower wear loss. It is also reported that the corrosion wear resistance of a material is related to passive film formed on its surface; a lower temperature may contribute to formation of a compact film in corrosive conditions (Ref 24, 25).

4.5 Effects of Film on Corrosion Wear

From the XPS spectra in Fig. 10 and 11, there are no Al or Fe peaks, which implies that dealuminum and deiron corrosion has been taken place on the Cu-14Al-X alloy surface and an ultrathin copper chloride [$CuCl_2 \cdot 3Cu(OH)_3$] and CuCl film has been formed on the corrosive surface (Ref 2, 18, 26).

Although bronzes are corrosion-resistant materials due to

Table 3 Worn track widths and corrosive weights of the Cu-14Al-X alloys

Media	Load, N	CA/Cu-14Al-X			HT/Cu-14Al-X		
		Corrosive wear loss, mg	Average scratching width, mm	Corrosive loss, mg	Corrosive wear loss, mg	Average scratching width, mm	Corrosive loss, mg
3.5 wt.% NaCl	15	0.5	0.56	1.2×10^{-3}	0.8	0.64	1.57×10^{-3}
	20	0.8	0.76	1.63×10^{-3}	1.2	0.69	1.7×10^{-3}
	24	1.0	0.90	1.94×10^{-3}	1.5	0.92	1.99×10^{-3}
	29	1.4	1.22	2.63×10^{-3}	1.9	0.95	2.05×10^{-3}

the formation of compact passive films, mechanical attack in the wear process breaks the protective films, thus the fresh surface is continuously exposed to a corrosive environment, resulting in an even worse situation than with normal passive surfaces. For Al bronzes, dealloying corrosion results in a noble copper subsurface, which has a passive function for further corrosion.

In addition, it was found that the hardness of the wear track surface was higher than that of the unworn surface (Fig. 9). This may be attributed to the strain hardening of the material. Strain hardening of the worn surface may improve the wear resistance of the material, in terms of the adhesive theory given by Archard (Ref 5, 22, 23). It is generally accepted that the wear loss is approximately inversely proportional to the hardness of the target material.

During the corrosive wear of the specimens in 3.5% NaCl solution, dealloying corrosion occurred and resulted in a passive patina or film on the specimen surface that prevented the surface from further corrosion. However, the patinas formed by corrosion would be broken down by the mechanical attack during the wear. As a result, a fresh surface was generated continuously in the wear process. The subsurface experienced plastic deformation during wear and exhibited strain hardening, which enhanced the surface hardness and thus increased the wear resistance.

5. Conclusions

Corrosion plays a trivial effect on the corrosion wear of aluminum bronzes in 3.5% sodium chloride solution. There is a "negative" synergy between corrosion and wear on the alloys.

The friction coefficient between bronzes and silicon nitride (Si_3N_4) ceramic in pure water is higher than that in dry sliding, but the wear loss is the opposite. Wear in air is a combined mode of plowing, delamination, and oxidation, while in water each of the behaviors becomes less severe.

Thermal conduction effects play an important role in the corrosion wear of the bronzes, as low temperature prevents the hardness of the surface from reducing, thus enhancing the wear resistance of the surface.

The bronzes suffered from dealloying corrosion, and a noble copper subsurface and patina that had a passive function for further corrosion had formed on the specimen surface. The subsurface experienced strain hardening during the sliding wear, which enhanced the surface hardness and thus increase the wear resistance.

Acknowledgments

This work was supported by Gansu Province Technology Bureau (grant no. GS992-A52-052) and was carried out with the help of Lanzhou Institute Chemical Physical and Institute of Metal Research, Chinese Academy of Sciences, in the experiments. The authors thank Dr. Rong Liu at Carleton University, Canada, for discussing the manuscript.

References

1. S. Alam, R.I. Marshall, and S. Sasaki, Metallurgical and Tribological Investigations of Aluminum Bronze Bushes Made by a Novel Centrifugal Casting Technique, *Tribol. Int.,* 1996, 29 (6), p 487-492
2. B.G. Ateya, E.A. Ashour, and S.M. Sayed, Stress Corrosion Behavior of α-Aluminum Bronze in Saline Water, *Corrosion: Corros. Sci.,* 1994, 50 (1), p 20-25
3. E. Stupnisek-Lisac, N. Galic, and R. Gasparac, Corrosion Inhibition of Copper in Hydrochloric Acid under Flow Conditions, *Corrosion: Corros. Sci. Sect.,* 2000, 56 (11), p 1105-1111
4. J.J. Wert, The Influence of Stacking Fault Energy and Adhesion on the Wear of Copper and Aluminum Bronze, *Wear,* 1988, 123, p 171-192
5. J.V. Reid and J.A. Schey, The Effect of Surface Hardness on Friction, *Wear,* 1987, 118, p 113-125
6. F.Z. Xiao and F. Liang, The Effect of Stacking Fault Energy on the Cavitation Erosion Resistance of α-Aluminum Bronzes, *Wear,* 2002, 253, p 1105-1110
7. Y.Y. Li, N.T. Leo, and W. Xia, Mechanical, Friction and Wear Behaviors of a Novel High-Strength Wear-Resisting Aluminum Bronze, *Wear,* 1996, 197, p 130-136
8. Z. Shi, Y. Sun, A. Bloyce, and T. Bell, Unlubricated Rolling-Sliding Wear Mechanisms of Complex Aluminum Bronze against Steel, *Wear,* 1996, 193, p 235-241
9. P.J. Blau, Investigation of the Nature of Micro-indentation Hardness Gradients below Sliding Contacts in Five Copper Alloys Worn against 52100 Steel, *J. Mater. Sci.,* 1957, 19, p 1957-1968
10. W.S Li, Z.P. Wang, Y. Lu, Y.H. Jin, L.H. Yuan, and F. Wang, Mechanical and Tribological Properties of a Novel Aluminum Bronze Material for Stretching and Squeezing Dies, *Wear,* in press
11. E.A. Ashour, E.A. Abd El Meguld, and B.G. Ateya, Stress Corrosion Behavior of Alpha Aluminum Bronze in Concentrated Alkali Solutions, *Corrosion: Corros. Sci. Sect.,* 2001, 57 (9), p 749-752
12. E.A. Ashour, Comparative Investigation of the Corrosion Behavior of Alpha Aluminum Bronze and Alpha Brass in Sodium Nitrite Solutions, *Proc. 2nd Int. Conf. on Heat Exchangers, Boilers, Pressure Vessels,* (Alexandria, Egypt), 1995, 37, p 371
13. R.N. Parkins and R.R. Fessler, Stress Corrosion Cracking of High-Pressure Gas Transmission Pipelines, *Int. J. Mater. Eng. Appl.,* 1978, 1 (2), p 80-96
14. J.H. Wang, X.X. Jiang, and S.Z. Li, Corrosive Wear Behavior of Copper Alloys in 3.5% NaCl+S^{2-} Solutions, *J. Chin. Soc. Corros. Protect.,* 1997, 17 (2), p 81-86, in Chinese
15. J.H. Wang, X.X. Jiang, and S.Z. Li, Corrosive Wear Behavior of Copper Alloys in 3.5% NaCl+$NH_3(NH_4^+)$ solution, *Acta Metall. Sin.,* 1997, 33 (12), p 1268-1274, in Chinese
16. T.C. Zhang, X.X. Jiang, X.C. Lu, and S.Z. Li, Quantitative Analysis of Synergy between Corrosion and Wear, *Chin. J. Mater. Res.,* 1994, 8 (5), p 397-401, in Chinese
17. J.F. Moulder, W.F. Stickle, P.D. Sobol, and K.D. Bomben, *Handbook of X-Ray Photoelectron Spectroscopy,* Physical Electronics, Inc., Eden Prairie, Minnesota, 1992
18. M.C. Squarcialupi, G.P. Bernardini, V. Faso, A. Atrei, and G. Rovida, Characterisation by XPS of the Corrosion Patina Formed on Bronze Surfaces, *J. Cult. Heritage,* 2003, 3, p 199-204

19. J.L. Sullivan and L.F. Wong, Wear of Aluminum Bronze on Steel under Condition of Boundary Lubrication, *Tribol. Int.,* 1985, 118 (5), p 275-281
20. R. Liu and D.Y. Li, Protective Effect of Yttrium Additive in Lubricants on Corrosive Wear, *Wear,* 1999, 225-229, p 969-974
21. T.C. Zhang and D.Y. Li, Improvement in the Resistance of Aluminum with Yttria Particles to Sliding Wear in Air and in a Corrosive Medium, *Wear,* 2001, 251, p 1250-1256
22. J.F. Archard, Contact and Rubbing of Flat Surface, *J. Appl. Phys.,* 1953, 24 (8), p 981-988
23. I.M. Hutchings, *Tribology: Friction and Wear of Engineering Materials,* Edward Arnold Press, London, 1992
24. J.L. Sullivan, Boundary Lubrication and Oxidation Wear, *J. Phys. D: Appl. Phys.,* 1986, 19 (10), p 1999-2011
25. A. Iwabuchi, T. Sonoda, H. Yashiro, and T. Shimizu, Application of Potential Pulse Method to the Corrosion Behavior of the Fresh Surface Formed by Scratching and Sliding in Corrosive Wear, *Wear,* 1999, 225-229, p 181-189
26. S.I. Gheyas, B.L. Strable, D.R. Strongin, and A.P. Wright, Cl_2 Surface Chemistry on Cu/Si (100): An ISS, XPS, and TPD Study, *Surf. Sci.,* 2001, 474 (1-3), p 129-138